The Design and Characterisation of Sinusoidal Toolpaths using Sub-Zero Bioprinting of Polyvinyl Alcohol

Gale, Lucie; Panieraki, Argyro; Mahmoodi, Nasim; Crolla, Joseph; Thomas-Seale, Lauren

DOI:
10.1016/j.jmbbm.2024.106402

Document Version
Publisher's PDF, also known as Version of record

Citation for published version (Harvard):
Gale, L, Panieraki, A, Mahmoodi, N, Crolla, J & Thomas-Seale, L 2024, 'The Design and Characterisation of Sinusoidal Toolpaths using Sub-Zero Bioprinting of Polyvinyl Alcohol', *Journal of the Mechanical Behavior of Biomedical Materials*, vol. 152, 106402. https://doi.org/10.1016/j.jmbbm.2024.106402

journal of the mechanical behavior of biomedical materials 152 (2024) 106402

Contents lists available at ScienceDirect

Journal of the Mechanical Behavior of Biomedical Materials

journal homepage: www.elsevier.com/locate/jmbbm

The design and characterisation of sinusoidal toolpaths using sub-zero bioprinting of polyvinyl alcohol

L. Gale, A. Panieraki, N. Mahmoodi, J.P. Crolla, L.E.J. Thomas-Seale *

Department of Mechanical Engineering, School of Engineering, University of Birmingham, UK

ARTICLE INFO

Keywords:
3D printing
Additive manufacturing
Bioprinting
Biomaterials
Computer aided manufacturing
Design

ABSTRACT

Sub-zero (°C) additive manufacturing (AM) systems present a promising solution for the fabrication of hydrogel structures with complex external geometry or a heterogeneous internal structure. Polyvinyl alcohol cryogels (PVA-C) are promising tissue-mimicking materials, with mechanical properties that can be designed to satisfy a wide variety of soft tissues. However, the design of more complex mechanical properties into additively manufactured PVA-C samples, which can be enabled using the toolpath, is a largely unstudied area. This research project will investigate the effect of toolpath variation on the elastic and viscoelastic properties of PVA-C samples fabricated using a sinusoidal toolpath. Samples were fabricated using parametric variation of a sinusoidal toolpath, whilst retaining the same overall cross-sectional area, using a sub-zero AM system. To mechanically characterise the samples, they were tested under tension in uniaxial ramp tests, and through dynamic mechanical analysis (DMA). The elastic and viscoelastic moduli of the samples are presented. No correlations between the parametric variation of the design and the Young's modulus were observed. Analysis of the data shows high intra-sample repeatability, demonstrated robust testing protocols, and variable inter-sample repeatability, indicating differences in the printability and consistency of fabrication between sample sets. DMA of the wavelength samples, show a frequency-dependent loss moduli. The storage modulus demonstrates frequency independence, and a large increase in magnitude as the sample increases to 3 wavelengths.

1. Introduction

Soft tissue damage is a growing issue worldwide (Marrella et al., 2018), with their poor self-repair properties often leading to the development of life-long conditions, significantly reducing patient quality of life (Krafts, 2010; Dell'accio et al., 2010; Wong et al., 2017). Prevalent examples include osteoarthritis, a prominent cause of disability worldwide (Liu et al., 2022), and cardiovascular disease, which is culpable for 25 % of deaths in England each year (BHF, 2023). Ongoing challenges with understanding and then replicating the hierarchal and inter-related structural, mechanical and biological functionality of soft tissues, mean that treatment options for such conditions are limited (Chanda and Callaway, 2018; Nasircilar et al., 2022). As such, the fabrication of materials that mimic the intrinsic complexity of material properties and mechanical behaviour of tissue, remains an active area of research. Polyvinyl alcohol (PVA) cryogels are promising tissue-mimicking materials, namely due to their mechanical properties akin to those of natural tissues (Su et al., 2019; Butylina et al., 2016), and the ability to alter their mechanical properties during fabrication. The extensive biomedical applications of cryogels, including PVA, are outlined in the review by Memic et al. (2019). Physical crosslinking of PVA cryogels (PVA-C) can be accomplished through freeze-thaw cycles (FTCs). During freezing, crystal nuclei form, which then grow into crystals during thawing; these crystals act as the polymer cross-links (Chu and Rutt, 1997). The number and duration of FTCs greatly affect the stiffness of the resultant cryogel (Gupta et al., 2012; Abdel-Mottaleb et al., 2009), where additional cycles create more cross-links forming a rubber-like gel (Chu and Rutt, 1997).

Traditional forming methods, such as casting, can limit the design of tissue mimicking materials, in terms of the complexity of the mould and the inherent isotropic properties. Additive manufacturing (AM) presents a promising technique to enable the fabrication of hydrogel structures with greater degrees of complexity (Weems et al., 2021). Extrusion-based AM systems achieve three-dimensional (3D) objects by building up layers of extruded material and offer a unique opportunity for the directional control of toolpaths in 3D (Uribe-Lam et al., 2021). Previous studies investigating the printability, have highlighted perpetuating challenges associated with fabricating hydrogel scaffolds

* Corresponding author. Department of Mechanical Engineering, School of Engineering, University of Birmingham, Edgbaston, B15 2TT, UK.
E-mail address: l.e.j.thomas-seale@bham.ac.uk (L.E.J. Thomas-Seale).

https://doi.org/10.1016/j.jmbbm.2024.106402
Received 4 October 2023; Received in revised form 10 January 2024; Accepted 11 January 2024
Available online 1 February 2024

using AM (Murphy and Atala, 2014). Namely, the low stiffness and viscous nature of hydrogels results in spreading upon deposition and an increased likelihood of 3D constructs collapsing under their own weight (Uribe-Lam et al., 2021). As such, further research is required to enable increased design complexity and retain high shape fidelity of hydrogel structures fabricated using AM.

The development of sub-zero (°C) AM systems has enhanced the printability of PVA hydrogels by achieving physical crosslinking, and forming PVA-C, upon deposition. Despite various studies reporting the success of using such sub-zero AM systems for fabricating hydrogel structures (Crolla et al., 2021a; Fischer et al., 2016), very limited work has been conducted to investigate the effect of toolpath on the resultant structural mechanical properties. Crolla et al. (2021a) studied the orthotropic characterisation of additively manufactured PVA-C using toolpaths parallel and perpendicular to the loading direction. However, the toolpath is not limited to commercial computer-aided manufacturing software and can customised manually or through computer aided design (CAD). Ji and Guvendiren (2019) report that compared to orthogonal scaffolds, wavy scaffolds of poly(caprolactone), result in significantly enhanced osteogenesis (Ji and Guvendiren, 2019). Gómez-Castañeda et al. (2023) explored the geometric parametrization of sinusoidal-based lattice polylactic acid (PLA) structures and subsequent tensile mechanical properties (Gómez-Castañeda et al., 2023). Both studies exploit the design freedom afforded by the parametric variation of wavelength and amplitude in the context of the scaffold or lattice function (Ji and Guvendiren, 2019; Gómez-Castañeda et al., 2023).

The aim of this study is to characterise solid additively manufactured PVA-C samples with sinusoidal toolpaths and explore the change in the elastic and viscoelastic mechanical response with the parametric variation of the wavelength and amplitude. The samples will be mechanically characterised, with respect to toolpath design, using uniaxial ramp testing and dynamic mechanical analysis (DMA).

2. Methods

2.1. Sample design

In this study, the toolpath was constrained by creating a CAD of the waves, with respect to the distance between the resolution of the deposited material and the distance between the filament lines. The samples were designed using SolidWorks (Dassault Systèmes, SolidWorks Corporation, Massachusetts, United States), based on a sinusoidal waveform with the variation of the amplitude (Testing Group 1) of 2 mm, 3 mm and 4 mm and number of wavelengths (Testing Group 2) of 1, 2 and 3. Fig. 1 shows examples of the design for each group of samples; where the height of the wave peaks are equivalent on each side of the sample. The dimensions labelled in black in the figure remained constant between samples as the sine wave amplitudes (marked as blue) and wavelengths were varied. The width of the samples (12.3 mm) was chosen to align with the width of the mechanical testing clamps. The additional 10 mm straight sections on either end of the samples provided clamping surfaces for the mechanical testing. Table 1 details the sine wave parameters of each sample and their respective sample numbers. Four samples of each type were manufactured, and were printed in one batch, as shown in Fig. 2(b). The samples were two layers (of 0.4 mm height) thick to ensure that the samples provided adequate thickness for gripping during testing whilst retaining the temperature accuracy perpendicular to the build platform.

2.2. Sample fabrication

An 11 % w/w PVA solution was prepared by dissolving powdered PVA, with a hydrolysis of 99+ % and molecular weight of 146–186 kDa (Sigma-Aldrich, Missouri, USA), in deionised (DI) water through autoclaving (1 h at 121 °C), and continuous mechanical stirring of the solution for 2 h – 1 h on a hotplate at 50 °C, followed by 1 h with the hotplate removed, allowing the solution to gradually return to ambient temperature.

To fabricate the samples, a REGEMAT Bio V1 bioprinter (REGEMAT, Granada, Spain) fitted with a 0.58 mm diameter nozzle was used (Fig. 2 (a)). The temperature of the glass bioprinter bed was maintained at −9.5 ± 0.5 °C during printing, to enable physical cross-linking of the PVA-C to occur upon deposition.

An .STL file exported from SolidWorks, was sliced using the REGEMAT3D Designer (REGEMAT, Granada, Spain) software to generate the G-code for the manufacture of the samples. Table 2 shows the process parameters used for the fabrication of the samples. These parameters were tailored during preliminary research to achieve printability for the specified material and toolpath design, with the intention of creating a solid sample.

To ensure the samples were sufficiently cross-linked to retain their structure, they were left on the printer bed for an additional 15 min after the completion of printing. The printed samples were then subjected to three further FTCs consisting of: 12 h in a freezer at −20 °C, 4 h in the freezer turned off and 8 h at ambient temperature. Upon the completion of the FTCs, the samples were stored in DI water at ambient temperature. The samples were mechanically tested after four days (uniaxial tensile

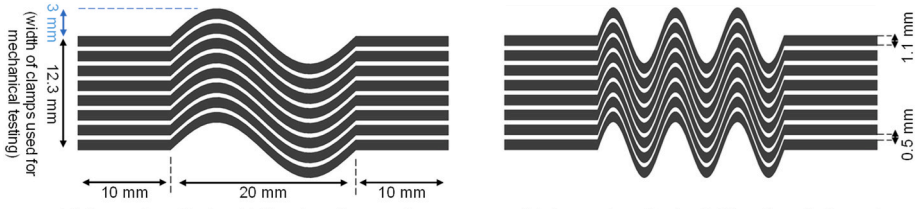

(a) 3 mm Amplitude, 1 Wavelength sample. (b) 3 mm Amplitude, 3 Wavelength Sample.

Fig. 1. Final sample designs.

Table 1
Sinusoidal parameters of the samples, and respective identifiers.

Testing Group	Sample Numbers	Amplitude (mm)	Number of wavelengths in 20 mm wavey portion
1	2.1, 2.2, 2.3, 2.4	2.00	1
1	3.1, 3.2, 3.3, 3.4	3.00	1
1	4.1, 4.2, 4.3, 4.4	4.00	1
2	λ1.1, λ1.2, λ1.3, λ1.4	3.00	1
2	λ2.1, λ2.2, λ2.3, λ2.4	3.00	2
2	λ3.1, λ3.2, λ3.3, λ3.4	3.00	3

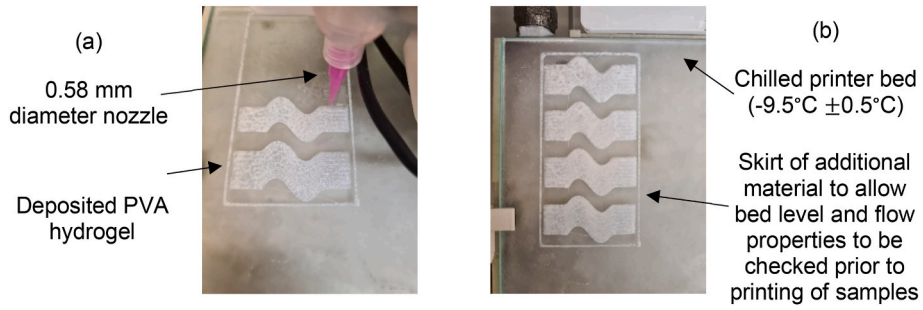

Fig. 2. Additive manufacture of PVA-hydrogel samples using a REGEMAT Bio V1 bioprinter (a) during printing, (b) after printing.

Table 2
Printing parameters used in conjunction with the REGEMAT Bio V1 bioprinter to manufacture the hydrogel samples.

Parameter	Value
Nozzle Diameter (mm)	0.58
Layer Height (mm)	0.40
Infill (%)	0
Flow Speed (mm/s)	0.6
Printing Speed (Extruding material) (mm/s)	2.0
Travel Speed (No material being extruded) (mm/s)	30.0
Retract Speed (mm/s)	30.0

ramp testing) and then seven days (DMA) of being stored in DI water.

2.3. Mechanical testing

All samples were mechanically tested using a Bose Electroforce 3200 (TA Instruments, Delaware, USA) and 250 g load cell (TA Instruments, Delaware, USA); the set-up is shown in Fig. 3. The mechanical properties of the samples were tested through a uniaxial tensile ramp test and DMA, with each test being repeated three times for each sample. Prior to mechanical testing, the width (taken across the portion to be clamped in the gripper) and thickness of each sample was measured using vernier callipers (Appendix A, Table A1).

To ensure the distance between the clamps remained constant across all samples, the clamps were set at 20 mm apart. The alignment of the clamps was checked to ensure only uniaxial tension was applied to the samples. When clamping the samples, care was taken to ensure that the clamps were not over-tightened (evidenced by the presence of bulging in the sample around the clamp jaws).

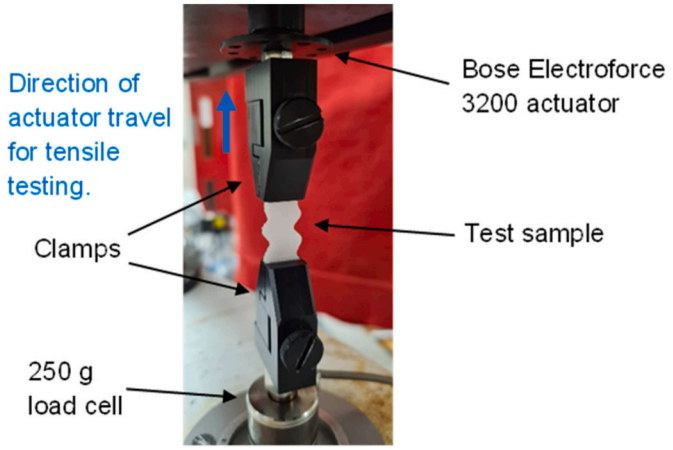

Fig. 3. Testing set-up for uniaxial tensile ramp testing on a Bose Electroforce 3200 mechanical testing machine.

2.3.1. Uniaxial tensile ramp testing

The samples were tested under tension to 20 % engineering strain (ε), at a rate of 0.25 mm/s. The required actuator displacement (d) to achieve 20 % engineering strain was calculated to be 4 mm (Equation (1)), where L is the sample length (20 mm). The engineering strain (ε) and stress (σ) for each sample and repeat were calculated using Equations (1) and (2), respectively, from the raw force (F) and displacement (d) data. The area (A) that the force was applied to was calculated using the thickness (T_c) and width (W_c) of the clamped portion of the samples (Equation (3)).

$$\varepsilon = \frac{d}{L} \quad \text{Eq.1}$$

$$\sigma = \frac{F}{A} \quad \text{Eq.2}$$

$$A = T_C \times W_C \quad \text{Eq.3}$$

The inter and intra variability of samples with the same sine wave parameters was investigated. Moreover, to explore the linearity of the data, the Young's Modulus was extracted at four different strain ranges: 4.5 %–5.5 %, 7.5 %–8.5 %, 11.5 %–12.5 % and 15.5 %–16.5 %.

2.3.2. Dynamic mechanical analysis

DMA was set-up in an identical manner to the tensile ramp tests, and a sinusoidal tensile load (dynamic amplitude 0.4 mm) with nine different frequency conditions (0.5–10 Hz) was applied to the samples. These frequencies were chosen as they align with previous studies on DMA of PVA-hydrogels (Crolla et al., 2021b; Crolla, 2022), and to simulate strain rates experienced by various soft tissues (Burton et al., 2016; Sadeghi et al., 2015; Schwartz and Bahadur, 2007). The strain range to test the samples between was selected based on the linear regions of the stress-strain curves, obtained from the ramp tests. The samples were tested between 13 % and 17 % strain (mean level = 3 mm, dynamic amplitude = 0.4 mm) as this was within the elastic region for the majority of samples (discussed further in Section 3.2.4). To limit sample dehydration, which could potentially alter the mechanical properties of the PVA-Cs (Li et al., 2020), the three repeats for each sample were not conducted consecutively. DMA was performed once for each sample, before moving onto the second repeat for each sample, then finally moving onto the third repeats. The samples remained in DI water when not being tested.

The method for characterising biomaterial viscoelastic properties, outlined by Lawless (2019) was used as the basis to analyse the DMA test data (Lawless, 2019). The dynamic stiffness (K^*), was obtained from a Fast Fourier Transform of the displacement (d) and load (F) data, Equation (4). The phase relationship between F and d (δ) yielded from the Fourier analysis was used to calculate the storage and loss stiffnesses (K' and K''), Equations (5) and (6). Each sample's shape factor (S) was calculated using their respective dimensions (width (W_C), thickness (T_C) and height (H)) and Equation (7). Finally, the storage and loss moduli (E' and E'') were calculated using Equations (8) and (9) respectively

(Lawless, 2019).

$$K^{*} = \frac{F}{d} \quad \text{Eq.4}$$

$$K' = K(\cos(\delta)) \quad \text{Eq.5}$$

$$K'' = K(\sin(\delta)) \quad \text{Eq.6}$$

$$S = \frac{W_C T_C}{H} \quad \text{Eq.7}$$

$$E' = \frac{K'}{S} \quad \text{Eq.8}$$

$$E'' = \frac{K''}{S} \quad \text{Eq.9}$$

2.4. Statistical analysis

One-way ANOVA tests at 95 % confidence level were conducted (Minitab, MINITAB, Pennsylvania, USA (Minitab, 2020)) to ascertain whether the differences between the mean mechanical properties of the samples or testing repetitions were statistically significant. Prior to DMA analysis, the linearity of the data was assessed using, two different statistical methods. Firstly, to ascertain if the Young's Modulus varied with strain, one-way ANOVA tests were carried out to test for statistical difference between the mean Young's Modulus for each sample type at the four strain ranges, performed at a 95 % confidence level. Additionally, linear and quadratic regression models were fitted to each sample for each repeat, and the resultant R^2 values were used to evaluate the fit of the models.

3. Results

3.1. Printability

A total of 24 samples were printed during this project. Despite the same printing parameters being used for all samples, the visual quality of the prints varied. It is hypothesised that this was due to fluctuations in the ambient temperature of the laboratory, further research is required to confirm this. Figures A1 to A24 in Appendix A show all the samples after the completion of the three FTCs. Out of the 24 samples, eight (Sample 2.1 to 3.4) had some separation between strands. One sample (Sample λ3.4) was discarded due to the nozzle clogging during printing (see Figure A24, Appendix A). The raw stress-strain graphs for each ramp test can be found in the supplementary data (SD), Figs. S1–S23.

3.2. Uniaxial tensile ramp testing results

3.2.1. Effect of toolpath variations on Young's modulus

The Young's Moduli were obtained from the gradients of the best-fit lines through a linear region (8 %–12 %) strain of the stress-strain curves. Fig. 4 shows the mean Young's Modulus for each sample type, calculated using the intra-repeats of the four specimens for each sample type. No correlation was identifiable between Young's Modulus and variation in amplitude or wavelengths. Samples with an amplitude of 3 mm and 1 wavelength, are equivalent designs (see Table 1) between testing group 1 and 2, yet have a notable different Young's Moduli; 3 A = 48,453 ± 3043 Pa and 1λ = 79,243 ± 10,507 Pa.

3.2.2. Inter-sample variability

The Young's Moduli data for each specimen of each sample type, including all repeats, is shown in Fig. 5. Samples 2.4 (Fig. 5(a)) and λ1.4 (Fig. 5(d)) yielded consistently lower and higher Young's Moduli (respectively) than the other specimens of the same sample type at each strain range. As such, these samples were assumed to be anomalous and removed from the ensuing analysis (discussed further in section 4.2.2).

A one-way ANOVA test was used to statistically assess the inter-sample variability, within the same strain range (Appendix B, Table B1). This analysis highlighted further differences between samples of the same type, although not at every strain range. Notably, three sample types (3 mm and 4 mm amplitude and 3λ) demonstrated statistically significant differences between samples at selected strain ranges.

3.2.3. Intra-sample variability

The Young's Modulus data for each repetition, was grouped by sample type (Fig. 6). From Fig. 6(f), Sample λ3.1 Rep 1 was identified as anomalous and was removed from further analysis, as it yielded a significantly lower Young's Modulus and a significantly greater standard deviation than the other repetitions for this sample type. This was confirmed by the stress-strain data, which shows that the sample slipped at approximately 15 % strain. Otherwise, Fig. 6 shows no identifiable between variations in the Young's Modulus and an increase in testing repetitions. A one-way ANOVA analysis was used to test the difference between the repeats of all sample types, at each strain region. Only one sample type showed a statistical difference between repeats: the 2λ samples at 4.5 %–5.5 % strain, where Rep 1 was found to be statistically different to Rep 3.

3.2.4. Linearity of stress-strain data

Fig. 7 and Table 3 show an example of the results from the performed statistical analyses, of all repeats, for one sample type (2 mm amplitude). The full statistical test results can be found in Tables B2 and B3 (Appendix B). From the one-way ANOVA tests, only two sample types were found to have a statistical difference between the Young's Moduli at the

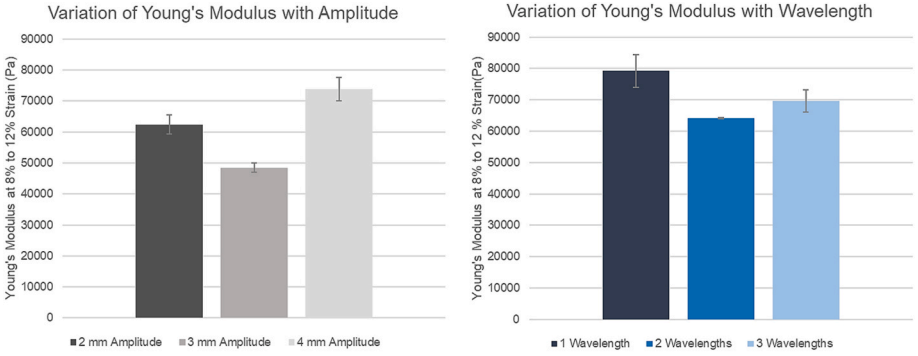

(a) Samples with varying amplitudes. (b) Samples with varying wavelengths.

Fig. 4. Young's Modulus at 8 %–12 % strain for each sample type. Error bars show the deviation between samples within each sample type (three repetitions per sample).

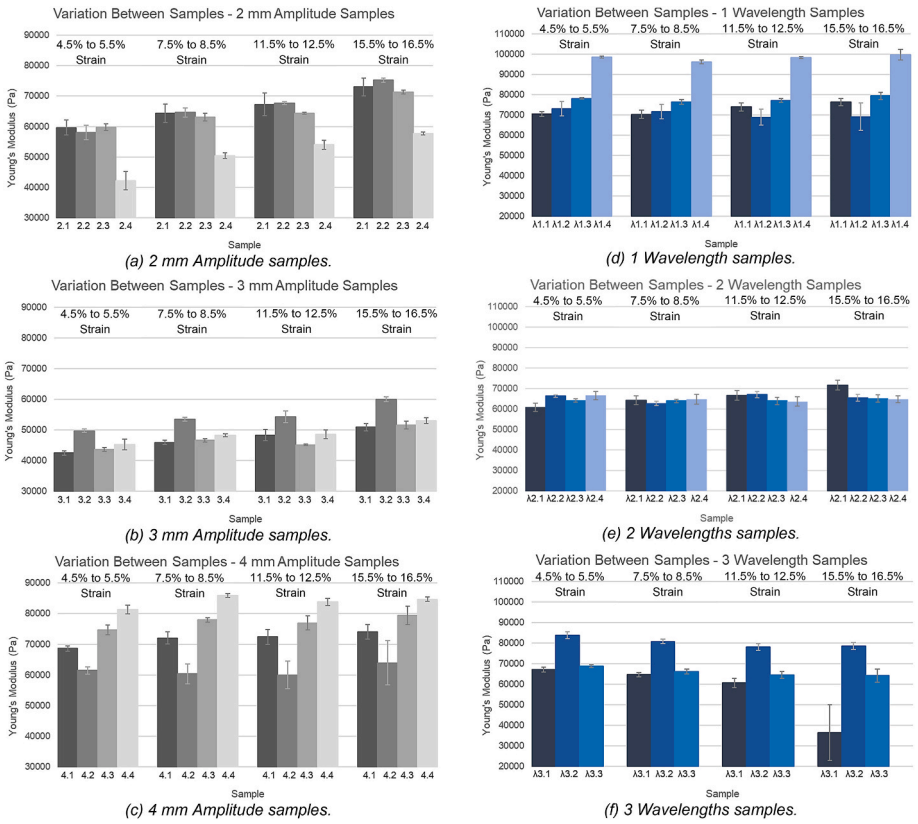

Fig. 5. Young's Modulus for different strain ranges (4.5 %–5.5 %, 7.5 %–8.5 %, 11.5 %–12.5 % and 15.5 %–16.5 %), for each sample (mean average of the three repeats) to show inter-sample variability. Error bars show the standard deviation of the three repeats.

four strain ranges: 2 A and 3 A. The regression analysis yielded linear model R^2 values of >99 % for all samples, except for Sample λ3.1 (linear model $R^2 = 97.83$ %).

3.3. Dynamic mechanical analysis results

DMA was performed on all samples. However, the ambiguity and consistency around the linearity of the stress-strain data (Section 3.2.4) should be acknowledged when viewing the data or generalising the conclusions of the study. For Sample 2.1 only the first repetition is included in the data analysis, due to sample dehydration. Fig. 8 shows the storage and loss moduli for all sample types. Similarly to the Young's Moduli data (Section 3.2.1), there is no clear trend of storage and loss modulus behaviour relative to amplitude or wavelength. All samples demonstrated an increase in loss modulus with increasing frequency. Predominately, the storage modulus appears independent of frequency, the exception being the 3 mm amplitude samples which demonstrate an increase in storage modulus across the frequency range. Similarly to the Young's moduli data (Section 3.2.1) the 3 mm amplitude samples yielded both the lowest storage and loss moduli. However, there was very little variation between the loss moduli with amplitude. For variation in wavelength, the 3λ samples yielded a significantly higher storage and loss moduli than the 1λ and 2λ samples. Less conclusive variation between sample types was observed for the loss modulus.

4. Discussion

4.1. Printability

It is hypothesised that the difference in sample print quality was due to variation in the ambient laboratory temperature, influenced largely by atmospheric temperature changes. As the viscosity of hydrogels is dependent on temperature (Etxabide et al., 2019; Kimbell et al., 2021), the degree of creep they exhibit post-extrusion varies with temperature. Consequently, the strand offset distances (identified in preliminary work) may only be optimised for the environmental conditions on that specific day. The 2 A and 3 A samples were printed on the same day and were the only samples to exhibit separation between strands, suggesting that ambient temperature was the cause. This hypothesis requires further research to confirm. Crolla et al. (2021a) reported that sub-zero AM introduces challenges with weak boundaries between extruded filament strands (Crolla et al., 2021a), which is in agreement with the visual observations made between filament strands in this research. The separation between strands for sample sets 2 A and 3 A may have affected the mechanical properties of the samples. This hypothesis is supported by the difference in average Young's moduli between sample groups 3 A and 1λ; whilst they have identical designs, they have significant different Young's Moduli. These sample sets were fabricated on different days, and have appreciably different print qualities, with the 3 A samples displaying separation between strands and consequently a lower stiffness.

4.2. Uniaxial tensile ramp testing results

4.2.1. Effect of toolpath variations on Young's modulus

As shown in Fig. 4, variations to the toolpath did not lead to an identifiable trend in the Young's moduli. For both Testing Groups, the middle sample type (3 A and 2λ) had the lowest Young's Modulus. Intuitively, it would be expected that increasing the amplitude and wavelength, would results in either an increase or decrease of Young's Moduli, neither of which were seen. To date, there is no literature on the fabrication and characterisation of wavey samples using sub-zero

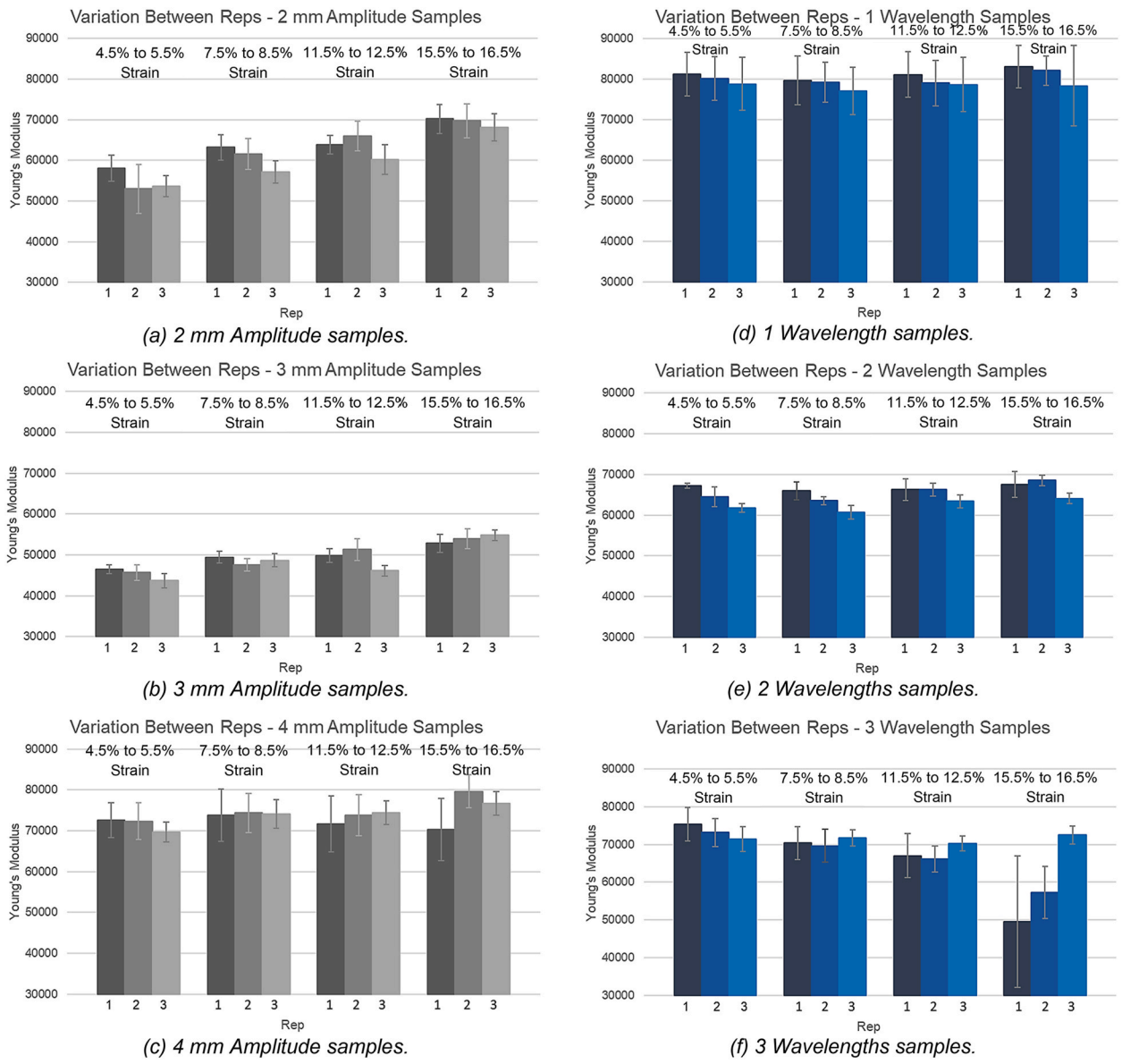

Fig. 6. Young's Modulus for different strain ranges (4.5 %–5.5 %, 7.5 %–8.5 %, 11.5 %–12.5 % and 15. %-16.5 %), for each repeat (mean average of the four samples) to show intra-sample variability. Error bars show the standard deviation of the four samples for each repeat.

bioprinting and comparison to similar studies is challenging to differences in methodology. Crolla et al. (2021a) and Chen et al. (2019) both found that directional dependent mechanical properties can be incorporated into PVA-hydrogel samples, although these studies used different sample designs and fabrication techniques (Crolla et al., 2021a; Chen et al., 2019). Gómez-Castañeda et al., 2023 explored the tensile response of sinusoidal-based lattice structures and found that the apparent Young's Modulus decreased non-linearly with increasing amplitude, however these were fabricated from thermoplastic PLA as opposed to a croygel (Gómez-Castañeda et al., 2023).

With reference to Fig. 9, increasing the amplitude and wavelength changes the sample in two ways; it increases the length of each toolpath/filament, it also increases the proportion of filament which is perpendicular to the loading direction. When the load is applied, because the composition of the sample is not isotropic, the change in the overall shape cannot be predicted. Whether such a load leads to straightening of the filament and/or elongation of the filament, or stretching and/or separation across the filament width is unknown. A combination of each behaviour is probable, depending on the vector decomposition of the load and the strength of the polymer bonds, within and between the filaments. Since the mechanical properties of PVA-C's are highly dependent on the physical cross-links formed through freezing, and there are differences in print quality (reported in Section 4.1), this would also depend on process parameters and environmental conditions. Further analysis is required through high-speed imaging of the deformation characteristics.

4.2.2. *Inter-sample and intra-sample variability*

The inter-sample and intra-sample variabilities were investigated to ascertain information about the repeatability of the testing and manufacturing processes. Splitting the data out by sample (Fig. 5) and repeat (Fig. 6) allowed anomalous results to be identified, and samples 2.4 and λ1.4, and Sample λ3.1 Rep 1 were removed from the subsequent sample variability analyses. The anomalous nature of Samples 2.4 and λ1.4 were caused by defects in the samples generated during fabrication; sample 2.4 displayed complete delamination of centre strands following

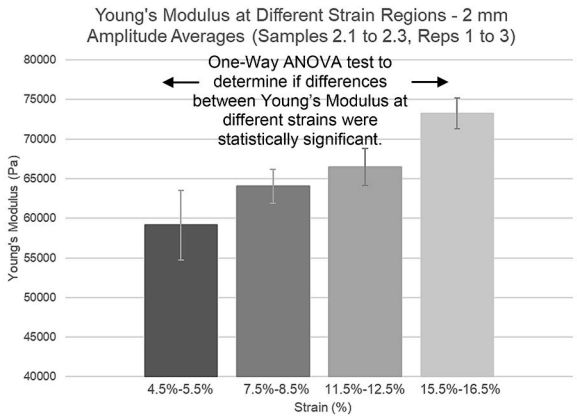

(a) One-Way ANOVA tests were performed to determine statistical signifcance between the Young's Modulus at different strain ranges. Error bars show the standard deviation of the three 2 mm Amplitude samples (Samples 2.1 to 2.3), including three testing repetitions per sample.

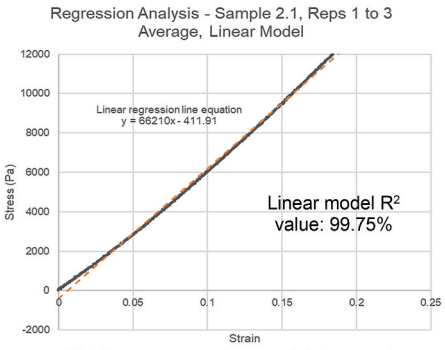

(b) Linear regression model (orange) superimposed on the raw stress-strain data (black) for Sample 2.1.

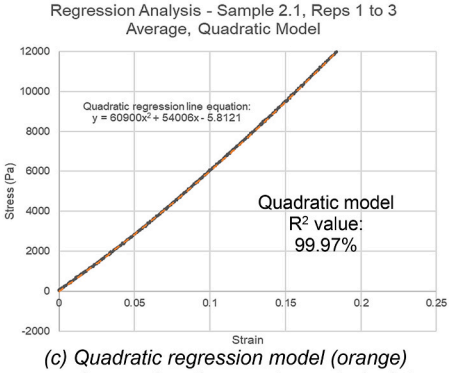

(c) Quadratic regression model (orange) superimposed on the raw stress-strain data (black) for Sample 2.1.

Fig. 7. Different statistical tests were employed to determine the linearity of the stress-strain data.

Table 3
Statistical analysis results for the 2 mm Amplitude samples.

Statistical Test	Result	Significance for determination of linearity
Regression analysis (Sample 2.1)	Linear Model R^2 value: 99.75 % Quadratic Model R^2 value: 99.97 %	The R^2 value for the quadratic model is greater than that for the linear model, suggesting that the quadratic model is a better fit for the data. However, the linear model still has an R^2 value above 99 %, showing that a linear model can also be considered a good fit for the data.
One-Way ANOVA (Sample 2.1, 2.2 and 2.3)	$p < 0.001$	$p < 0.05$, meaning that there are statistical differences between means: • 15.5 %–16.5 % strain is statistically different to 4.5 %–5.5 %, 7.5 %–8.5 % and 11.5 %–12.5 % strain. • 4.5 %–5.5 % is statistically different to 11.5 %–12.5 % strain. The one-way ANOVA test suggests that the data is not linear as there are statistical differences between the Young's Moduli at different strains along the stress-strain curve.

printing and sample λ1.4 experienced partial delamination of the first and second print layers when it was removed from the print bed (Figures A4 and A16, Appendix A). Reviewing the stress-strain curve for Sample λ3.1 Rep 1 (see SD Fig. S21), showed a significant decrease in the stress at approximately 15 % strain, indicating that this sample slipped in the clamps during testing.

The analysis of the inter-sample variability, showed some statistically significant differences between the means of some sample types at a fixed strain. These differences were isolated to 3 sample types (3 mm and 4 mm amplitude and 3λ) which suggests that the cause of these differences was between batches as opposed to within the same batch. As previously discussed, this is likely to be caused environmental parameters during the fabrication of these sets. To ascertain whether performing multiple testing repetitions resulted in plastic deformation or sample damage, the intra-sample variability was investigated. The lack of intra-sample variability suggests that the samples were not damaged/deformed due to testing and that the data for all testing repeats can be considered reliable and comparable.

4.2.3. Linearity of stress-strain data

Assessing linearity of the data between strain ranges, using ANOVA tests and regression analysis, yielded different conclusions, and thus the linearity of the data obtained in this study remains ambiguous. It is important to acknowledge this, when considering the validity of the DMA data for the sample sets that demonstrate non-linear characteristics. Predominately linear stress-strain data, between 0 and 20 %, strain

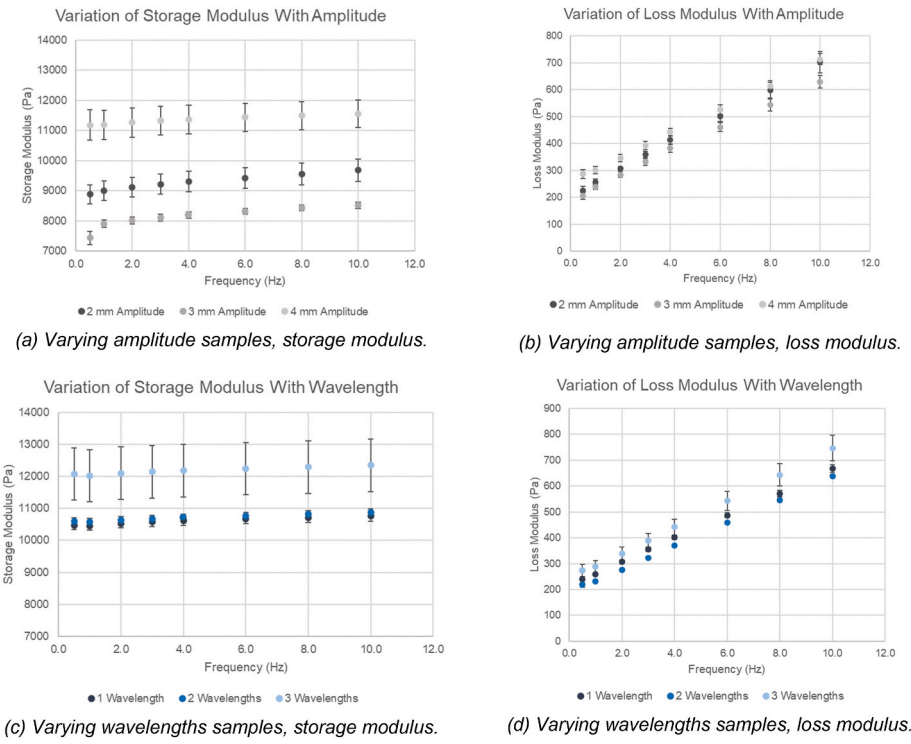

(a) Varying amplitude samples, storage modulus.

(b) Varying amplitude samples, loss modulus.

(c) Varying wavelengths samples, storage modulus.

(d) Varying wavelengths samples, loss modulus.

Fig. 8. Storage and the loss modulus for the samples with varying amplitudes, (a) and (b), and with varying wavelengths, (c) and (d). The error bars show the deviation between the samples within the respective sample type (all three repetitions per sample).

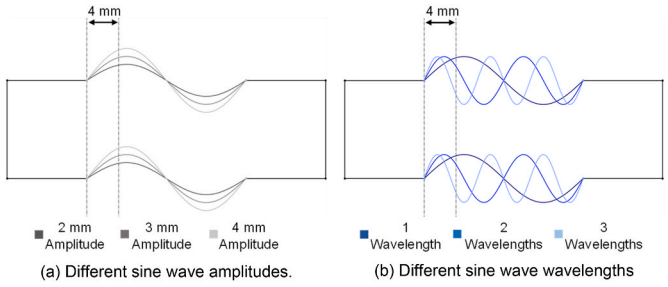

(a) Different sine wave amplitudes.

(b) Different sine wave wavelengths

Fig. 9. Diagrams showing all the sine wave parameter variations (i.e. the different amplitude and number of wavelengths used) for each sample type, with respect to the 4 mm tensile ramp test displacement distance.

for PVA-C samples has also been reported in other studies (Chen et al., 2019; Millon and Wan, 2006; Stammen et al., 2001; Wan et al., 2002), thus verifying the observations made about the data linearity. However, after approximately 20 % strain, these studies also reported a decrease in linearity with an increase in strain (Chen et al., 2019; Millon and Wan, 2006; Stammen et al., 2001; Wan et al., 2002). This divergence from linearity after a critical strain, is reported to be caused by the strain-stiffening behaviour of PVA-Cs, which occurs at relatively low strains, similar to many natural tissues (Millon and Wan, 2006; Wan et al., 2002; Destrade et al., 2009).

4.3. Dynamic mechanical analysis

DMA needs to be performed within the linear elastic region of a material to ensure that permanent deformation does not occur whilst the repeated sinusoidal load is applied (Patra et al., 2020). The samples were tested between 13 % and 17 % strain as during the experimental testing period, this strain range was nominally identified to be within the elastic region of the stress-strain curves for most samples. Following the further analysis of the linearity of the stress-strain data, the linearity of data for the 2 A and 3 A samples and Sample λ3.1 was inconclusive. Further to these, sample types 3 A, 4 A and 3λ were shown to have significant difference between the means at fixed strain. It was concluded that drawing any trends across Testing Group 1, would be unreliable. Within Testing group 2, sample set 3λ showed some difference between the means of 4.5 %–5.5 % and 7.5 %–8.5 %, and regression analysis was $R^2 = 97.83$ for a linear fit. Since DMA was conducted at 13 %–17 %, this was considered to be acceptable to proceed.

There was negligible variation between the storage moduli for the 1λ and 2λ samples. The 3λ samples yielded much high storage moduli across all frequencies, meaning that more input energy was required to distort these samples. This may be due to the presence of more wavelengths in the sample leading to a higher strain per wavelength, greater resistance to distortion and a greater ability to store elastic energy. Less variability was observed for the loss moduli between the wavelength samples, showing that the samples all displayed similar viscous properties, despite their different toolpath parameters.

All samples exhibited a marginal increase in the storage moduli (average increase of 2.6 % ± 0.3 %) and a significant increase in the loss moduli (average increase of 181.6 %± 7.9 %) across the frequency range. These trends agree with those found by Crolla et al. (2021a) when performing DMA on 10 % w/w additively manufactured sub-zero PVA-C samples (Crolla et al., 2021a). The storage moduli values for the samples in Testing Group 2 were greater than those reported for rectangular specimens with toolpaths parallel and perpendicular to the loading direction (Crolla et al., 2021a). This observed difference may be due to the differences in the fabrication methodology, or they could suggest that samples with sinusoidal toolpaths may yield a greater resistance to distortion.

4.4. Study limitations

There are many challenges with the AM of hydrogels which are associated with the low stiffness, variable viscosity and subsequent lack of shape fidelity; this study utilised a sub-zero AM platform to enable the PVA to physically crosslink (and thus retain its shape) upon deposition. It should be noted that whilst the printing platform was maintained at -9.5 ± 0.5 °C, any distance above the platform would be subject to interactions with the ambient temperature, which would influence the rate of the initial gelation process. This study characterised the mechanical properties of additively manufactured PVA-C with sinusoidal toolpaths which were designed manually, however there are other automated approaches to enable the customisation of toolpaths such as FullControl GCode Designer (Gleadall, 2021).

With respect to the aim, the Youngs, storage and loss moduli demonstrated no identifiable trend with amplitude or wavelength, the loss modulus showed a dependence on frequency. In this study, only three values of each parameter were studied, which is not sufficient to identify more complicated trends (such as parabolic) which may exist. To identify the source of the changes in the mechanical response, the internal behaviour of the polymer network, as a result of the fabrication technique, sample design and characterisation methodology requires further investigation. The change in the molecular structure of the PVA and arrangement of the water molecules, post-fabrication and pre and post mechanical characterisation, could be investigated through the Raman Spectra (Kudo et al., 2014).

In this study, the samples were only tested to 20 % strain. It is hypothesised that this was not a high enough strain for the differing toolpaths to demonstrate a significant effect. A displacement of 4 mm, and that distance relative to the design of the samples is shown in Fig. 9. Previous studies have found that the stress-strain relationship for PVA-Cs increases exponentially after approximately 20 % strain (Chen et al., 2019; Millon and Wan, 2006; Stammen et al., 2001; Wan et al., 2002). Additionally, Crolla et al. (2021a) found that differences in mechanical properties with varying toolpaths were greater with smaller nozzle sizes (Crolla et al., 2021a). This project used a nozzle diameter of 0.58 mm, potentially reducing the directional dependency of the samples' mechanical properties. During the uniaxial ramp tests, to ascertain the repeatability of the testing and manufacturing processes, the deformation needed to remain in the elastic region, as such the samples could not be tested to yield or ultimate strength.

During this study, samples were stored in DI water when not being tested. However, the effect of repeated sample dehydration and rehydration was not fully explored and requires further investigation in the context of the repeated mechanical characterisation. Kudo et al. (2014) demonstrate the use of Raman Spectroscopy to identify the changes in the polymer network and behaviour of water with cross-linking method, dehydration and reswelling (Kudo et al., 2014). The application of repeated strain may induce changes to the polymer network, which in the context of variable (an unknown dehydration rate during testing) and repeated water saturation (storage in DI water and subsequent reswelling), could influence the mechanical response of the sample. Furthermore, in future research a temperature and humidity-controlled environment should be used to investigate the impact of ambient conditions on printability and testing.

5. Conclusion

This research demonstrates how varying sinusoidal toolpath design, changes the mechanical properties of additively manufactured PVA-C. To achieve different toolpaths to fabricate samples of the same overall profile, sine wave toolpaths of differing amplitudes and wavelengths were designed. The mean Young's moduli with wavelength and amplitude are presented, from which the statistical significance between the inter- and intra-sample means are explored. Intra-sample differences demonstrated repeatable testing protocols. The inter-sample differences highlight sample sets, within which, statistically significant differences could be seen. Since the samples sets were printed in one batch on the same day, the effect of environmental changes needs to be explored in future research. The linearity of the data was explored across the strain range; whilst the samples with varying amplitude (testing group 1) gave ambiguous results, the majority of the data sets from samples with varying wavelength (testing group 2), showed linear characteristics. The DMA results of testing group 2, showed that whilst the loss moduli demonstrated frequency dependence, the storage moduli did not. The samples with 3λ, showed a large increase in storage moduli above those for the samples with 1λ and 2λ.

CRediT authorship contribution statement

L. Gale: Writing – original draft, Visualization, Validation, Project administration, Methodology, Investigation, Formal analysis, Data curation. **A. Panieraki:** Writing – review & editing, Supervision, Methodology, Data curation. **N. Mahmoodi:** Writing – review & editing, Supervision, Methodology, Data curation. **J.P. Crolla:** Methodology. **L. E.J. Thomas-Seale:** Writing – review & editing, Validation, Supervision, Resources, Methodology, Funding acquisition, Formal analysis, Conceptualization.

Declaration of competing interest

The authors declare that they have no known competing financial interests or personal relationships that could have appeared to influence the work reported in this paper.

Data availability

Data will be made available on request.

Acknowledgements

Funding: This work was supported by the Engineering and Physical Sciences Research Council [grant number EP/S036717/1]; and a School of Engineering, University of Birmingham, PhD Scholarship. The equipment used in this study was funded by Arthritis Research United Kingdom (grant number H0671; now part of Versus Arthritis)

Appendix A. Supplementary data

Supplementary data to this article can be found online at https://doi.org/10.1016/j.jmbbm.2024.106402.

Appendix A1

Table A1
Mean and standard deviation measurement data of three measurements taken from the same sample, and the mean and standard deviation of all measurements of all samples of the same design.

Sample Number(s)	Thickness (mm)		Width (mm)	
	Mean	Standard Deviation	Mean	Standard Deviation
Testing Group 1 – Differing Amplitudes				
2.1	0.93	0.01	10.97	0.03
2.2	0.91	0.01	11.03	0.04
2.3	0.97	0.02	10.57	0.05
2.4	0.98	0.02	11.09	0.04
2.1–2.4	**0.95**	**0.03**	**10.92**	**0.21**
3.1	1.09	0.03	12.06	0.06
3.2	0.99	0.02	11.11	0.02
3.3	0.98	0.03	10.99	0.02
3.4	0.99	0.02	11.14	0.05
3.1–3.4	**1.01**	**0.05**	**11.33**	**0.43**
4.1	0.97	0.01	11.35	0.10
4.2	0.96	0.02	12.11	0.10
4.3	0.97	0.01	11.14	0.04
4.4	0.93	0.02	11.18	0.08
4.1–4.4	**0.96**	**0.02**	**11.45**	**0.40**
Testing Group 2 – Differing Wavelengths				
λ1.1	0.92	0.00	11.17	0.06
λ1.2	0.90	0.01	11.10	0.06
λ1.3	0.87	0.02	10.92	0.02
λ1.4	0.82	0.02	11.11	0.03
λ1.1 - λ1.4	**0.88**	**0.04**	**11.07**	**0.11**
λ2.1	1.00	0.02	10.86	0.01
λ2.2	0.96	0.00	11.04	0.08
λ2.3	1.00	0.05	10.99	0.02
λ2.4	0.98	0.01	11.30	0.04
λ2.1 - λ2.4	**0.98**	**0.03**	**11.05**	**0.17**
λ3.1	1.01	0.02	11.46	0.03
λ3.2	1.00	0.03	11.06	0.02
λ3.3	1.05	0.02	11.38	0.05
λ3.4	N/A	N/A	N/A	N/A
λ3.1 - λ3.3	**1.02**	**0.03**	**11.30**	**0.18**

Fig. A1. Sample 2.1.

Fig. A2. Sample 2.2.

Fig. A3. Sample 2.3.

Fig. A4. Sample 2.4.

Fig. A5. Sample 3.1.

Fig. A6. Sample 3.2.

Fig. A7. Sample 3.3.

Fig. A8. Sample 3.4.

Fig. A9. Sample 4.1.

Fig. A10. Sample 4.2.

Fig. A11. Sample 4.3.

Fig. A12. Sample 4.4.

Fig. A13. Sample λ1.1.

Fig. A14. Sample λ1.2.

Fig. A15. Sample λ1.3.

Fig. A16. Sample λ1.4.

Fig. A17. Sample λ2.1.

Fig. A18. Sample λ2.2.

Fig. A19. Sample λ2.3.

Fig. A20. Sample λ2.4.

Fig. A21. Sample λ3.1.

Fig. A22. Sample λ3.2.

Fig. A23. Sample λ3.3.

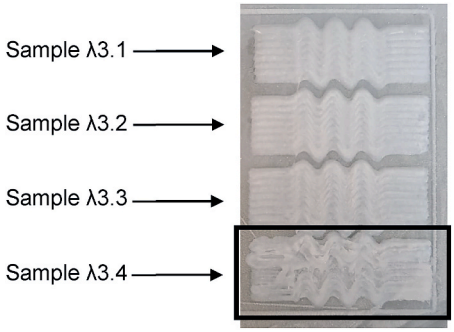

Fig. A24. Sample λ3.4 had to be discarded after printing due to the printer nozzle clogging during printing. All samples were imaged after 3FTCs.

Appendix B

Table B1
Results from one-way ANOVA tests (95 % confidence level) investigating inter-sample variability.

Strain Range	p-value	Test for a statistical difference between sample means
Inter-Sample Variability of 2 mm Amplitude Samples (2.1, 2.2 and 2.3)		
4.5 %–5.5 %	0.907	$p > 0.05$, therefore no statistical differences between means.
7.5 %–8.5 %	0.884	$p > 0.05$, therefore no statistical differences between means.
11.5 %–12.5 %	0.075	$p > 0.05$, therefore no statistical differences between means.
15.5 %–16.5 %	0.143	$p > 0.05$, therefore no statistical differences between means.
Inter-Sample Variability of 3 mm Amplitude Samples (3.1, 3.2, 3.3 and 3.4)		
4.5 %–5.5 %	0.018	$p < 0.05$, there are statistical differences between means: • Sample 3.2 is statistically different to Samples 3.1 and 3.3
7.5 %–8.5 %	0.015	$p < 0.05$, there are statistical differences between means: • Sample 3.2 is statistically different to Samples 3.1, 3.2 and 3.3
11.5 %–12.5 %	0.137	$p > 0.05$, therefore no statistical differences between means.
15.5 %–16.5 %	0.029	$p < 0.05$, there are statistical differences between means: • Sample 3.2 is statistically different to Sample 3.1
Inter-Sample Variability of 4 mm Amplitude Samples (4.1, 4.2, 4.3 and 4.4)		
4.5 %–5.5 %	0.008	$p < 0.05$, there are statistical differences between means: • Sample 4.1 is statistically different to Sample 4.4 • Sample 4.2 is statistically different to Samples 4.3 and 4.4
7.5 %–8.5 %	0.008	$p < 0.05$, there are statistical differences between means:

(*continued on next page*)

Table B1 (*continued*)

Strain Range	p-value	Test for a statistical difference between sample means
		• Sample 4.1 is statistically different to Sample 4.4
11.5 %–12.5 %	0.069	$p > 0.05$, therefore no statistical differences between means.
15.5 %–16.5 %	0.147	$p > 0.05$, therefore no statistical differences between means.
Inter-Sample Variability of 1 Wavelength Samples (λ1.1, λ1.2 and λ1.3)		
4.5 %–5.5 %	0.063	$p > 0.05$, therefore no statistical differences between means.
7.5 %–8.5 %	0.391	$p > 0.05$, therefore no statistical differences between means.
11.5 %–12.5 %	0.418	$p > 0.05$, therefore no statistical differences between means.
15.5 %–16.5 %	0.582	$p > 0.05$, therefore no statistical differences between means.
Inter-Sample Variability of 2 Wavelengths Samples (λ2.1, λ2.2, λ2.3 and λ2.4)		
4.5 %–5.5 %	0.403	$p > 0.05$, therefore no statistical differences between means.
7.5 %–8.5 %	0.873	$p > 0.05$, therefore no statistical differences between means.
11.5 %–12.5 %	0.798	$p > 0.05$, therefore no statistical differences between means.
15.5 %–16.5 %	0.514	$p > 0.05$, therefore no statistical differences between means.
Inter-Sample Variability of 3 Wavelengths Samples (λ3.1, λ3.2 and λ3.3)		
4.5 %–5.5 %	0.050	$p < 0.05$, there are statistical differences between means: • Sample λ3.2 is statistically different to Samples λ3.1 and λ3.3
7.5 %–8.5 %	0.026	$p < 0.05$, there are statistical differences between means: • Sample λ3.2 is statistically different to Sample λ3.3
11.5 %–12.5 %	0.057	$p > 0.05$, therefore no statistical differences between means.
15.5 %–16.5 %	0.196	$p > 0.05$, therefore no statistical differences between means.

Table B2
Results from one-way ANOVA tests (95 % confidence level) investigating data linearity by checking for a statistical difference between the Young's Modulus values at the different strain ranges (4.5–5.5 %, 7.5 %–8.5 %, 11.5 %–12.5 % and 15.5 %–16.5 %).

Sample Type	p-value	Statistical Difference Between Young's Modulus Means at Different Strain Ranges?
2 mm Amplitude	$p < 0.001$	$p < 0.05$, there are statistical differences between means: • 15.5 %–16.5 % strain is statistically different to 4.5 %–5.5 %, 7.5 %–8.5 % and 11.5 %–12.5 % % strain. • 4.5 %–5.5 % is statistically different to 11.5 %–12.5 % strain.
3 mm Amplitude	$p < 0.001$	$p < 0.05$, there are statistical differences between means: • 15.5 %–16.5 % strain is statistically different to 4.5 %–5.5 % and 7.5 %–8.5 % strain.
4 mm Amplitude	0.798	$p > 0.05$, therefore no statistical differences between means.
1 Wavelength	0.953	$p > 0.05$, therefore no statistical differences between means.
2 Wavelengths	0.350	$p > 0.05$, therefore no statistical differences between means.
3 Wavelengths	0.644	$p > 0.05$, therefore no statistical differences between means.

Table B3
Linear and quadratic R^2 values for the average stress-strain data (average of Reps 1 to 3) for each sample.

Sample	Linear Model R^2 Value (%)	Quadratic Model R^2 Value (%)
2.1	99.75	99.97
2.2	99.77	99.99
2.3	99.76	99.99
2.4	99.77	99.98
3.1	99.77	99.99
3.2	99.79	99.93
3.3	99.79	99.93
3.4	99.93	99.99
4.1	99.94	99.96
4.2	99.98	99.98
4.3	99.85	99.86
4.4	99.99	99.99
λ1.1	99.93	99.98
λ1.2	99.76	99.88
λ1.3	99.97	99.98
λ1.4	99.99	99.99
λ2.1	99.48	99.8
λ2.2	99.98	99.98
λ2.3	99.98	99.99
λ2.4	99.98	99.99
λ3.1	97.83	99.09
λ3.2	99.99	99.99
λ3.3	99.98	99.99

References

Abdel-Mottaleb, M.M., Mortada, N.D., El-Shamy, A.A., Awad, G.A., 2009. Physically cross-linked polyvinyl alcohol for the topical delivery of fluconazole. Drug Dev. Ind. Pharm. 35 (3), 311–320. https://doi.org/10.1080/03639040802325893.

BHF, 2023. Facts and Figures [Internet]. British Heart Foundation [cited 2023 Apr 27]. https://www.bhf.org.uk/what-we-do/news-from-the-bhf/contact-the-press-office/facts-and-figures#:~:text=Heart%20and%20circulatory%20diseases%20cause,men%20and%203.6%20million%20women.

Burton, H.E., Freij, J.M., Espino, D.M., 2016. Dynamic viscoelasticity and surface properties of porcine left anterior descending coronary arteries. Cardiovasc. Eng. Technol. 8 (1), 41–56. https://doi.org/10.1007/s13239-016-0288-4.

Butylina, S., Geng, S., Oksman, K., 2016. Properties of AS-prepared and freeze-dried hydrogels made from poly(vinyl alcohol) and cellulose nanocrystals using freeze-thaw technique. Eur. Polym. J. 81, 386–396. https://doi-org.bham-ezproxy.idm.oclc.org/10.1016/j.eurpolymj.2016.06.028.

Chanda, A., Callaway, C., 2018. Tissue anisotropy modeling using soft composite materials. Appl. Bionics Biomech. 2018 https://doi.org/10.1155/2018/4838157.

Chen, Y., Jiao, C., Peng, X., Liu, T., Shi, Y., Liang, M., et al., 2019. Biomimetic anisotropic poly(vinyl alcohol) hydrogels with significantly enhanced mechanical properties by freezing–thawing under drawing. J. Mater. Chem. B 7 (20), 3243–3249. https://doi.org/10.1039/c9tb00372j.

Chu, K.C., Rutt, B.K., 1997. Polyvinyl alcohol cryogel: an ideal phantom material for mr studies of arterial flow and elasticity. Magn. Reson. Med. 37 (2), 314–319. https://doi.org/10.1002/mrm.1910370230.

Crolla, J.P., 2022. Replicating the Intrinsic Biomechanical Characteristics of Connective Tissue: an Exploration into the Design and Manufacture of PVA Cryogel. Thesis, University of Birmingham.

Crolla, J.P., Britton, M.M., Espino, D.M., Thomas-Seale, L.E.J., 2021a. The orthotropic viscoelastic characterisation of sub-zero 3D-printed poly(vinyl alcohol) cryogel. MRS Adv 6 (18), 467–471. https://doi.org/10.1557/s43580-021-00086-1.

Crolla, J.P., Britton, M.M., Espino, D.M., Thomas-Seale, L.E.J., 2021b. The dynamic viscoelastic characterisation and magnetic resonance imaging of poly(vinyl alcohol) Cryogel: identifying new attributes and opportunities. Mater. Sci. Eng. C 129. https://doi.org/10.1016/j.msec.2021.112383.

Dell'accio, F., Vincent, T.L., 2010. Chapter 5 - understanding tissue response to cartilage injury. In: Archer, C., Ralph, J. (Eds.), Regenerative Medicine and Biomaterials for the Repair of Connective Tissues. Woodhead Publishing, pp. 137–154.

Destrade, M., Ní Annaidh, A., Coman, C.D., 2009. Bending instabilities of soft biological tissues. Int. J. Solid Struct. 46 (25), 4322–4330. https://doi.org/10.1016/j.ijsolstr.2009.08.017.

Etxabide, A., Long, J., Guerrero, P., de la Caba, K., Seyfoddin, A., 2019. 3D printed lactose-crosslinked gelatin scaffolds as a drug delivery system for Dexamethasone. Eur. Polym. J. 114 (1), 90–97. https://doi-org.bham-ezproxy.idm.oclc.org/10.1016/j.eurpolymj.2019.02.019.

Fischer, B., Schulz, A., Gepp, M.M., Neubauer, J., Gentile, L., Zimmermann, H., 2016. 3D printing of hydrogels in a temperature controlled environment with high spatial resolution. CDBME 2 (1), 109–112. https://doi.org/10.1515/cdbme-2016-0027.

Gleadall, A., 2021. FullControl GCode Designer: Open-source software for unconstrained design in additive manufacturing. Addit. Manuf. 46, 102109. https://doi.org/10.1016/j.addma.2021.102109.

Gómez-Castañeda, M., Cuan-Urquizo, E., Giraldo-Betancur, A.L., Félix-Martínez, C., Gómez-Ortega, A., Alvarado-Orozco, J.M., 2023. Additive manufacturing and mechanical characterization of sinusoidal-based lattice structures: a numerical and experimental approach. Prog. Addit. Manuf. https://doi.org/10.1007/s40964-023-00453-4.

Gupta, S., Sinha, A., Goswami, S., 2012. A combined effect of freeze-thaw cycles and polymer concentration on the structure and mechanical properties of transparent PVA gels. Biomed. Mater. 7 (1) https://doi.org/10.1088/1748-6041/7/1/015006.

Ji, S., Guvendiren, M., 2019. 3D printed wavy scaffolds enhance mesenchymal stem cell osteogenesis. Micromachines 11 (1), 31. https://doi.org/10.3390/mi11010031.

Kimbell, G., Azad, M.A., Nurunnabi, M., 2021. Chapter FIFTEEN - 3D printing: bioinspired materials for drug delivery. In: Bioinspired and Biomimetic Materials for Drug Delivery. Woodhead Publishing, Oxford, pp. 295–318.

Krafts, K.P., 2010. Tissue repair: the hidden drama. Organogenesis 6 (4), 225–233. https://doi.org/10.4161/2Forg.6.4.12555.

Kudo, K., Ishida, J., Syuu, G., Sekine, Y., Ikeda-Fukazawa, T., 2014. Structural changes of water in poly(vinyl alcohol) hydrogel during dehydration. J. Chem. Phys. 140 (4) https://doi.org/10.1063/1.4862996.

Lawless, B., 2019. Biostability of an Orthopaedic Device and its Long-Term Implantable Biomaterials. Thesis, University of Birmingham.

Li, Z., Liu, Z., Ng, T.Y., Sharma, P., 2020. The effect of water content on the elastic modulus and fracture energy of hydrogel. EML 35. https://doi-org.bham-ezproxy.idm.oclc.org/10.1016/j.eml.2019.100617.

Liu, M., Jin, F., Yao, X., Zhu, Z., 2022. Disease burden of osteoarthritis of the knee and hip due to a high body mass index in China and the USA: 1990–2019 findings from the global burden of disease study 2019. BMC Muscoskel. Disord. (63), 23. https://doi.org/10.1186/s12891-022-05027-z.

Marrella, A., Lagazzo, A., Dellacasa, E., Pasquini, C., Finocchio, E., Barberis, F., et al., 2018. 3D porous gelatin/PVA hydrogel as meniscus substitute using alginate micro-particles as porogens. Polym. J. 10 (4), 380–396. https://doi.org/10.3390/polym10040380.

Memic, A., Colombani, T., Eggermont, L.J., Rezaeeyazdi, M., Steingold, J., Rogers, Z.J., et al., 2019. Latest advances in cryogel technology for biomedical applications. Adv. Ther. 2 (4) https://doi.org/10.1002/adtp.201800114.

Millon, L.E., Wan, W.K., 2006. The polyvinyl alcohol–bacterial cellulose system as a new nanocomposite for biomedical applications. J. Biomed. Mater. Res. Part B App. Biomater. 79B (2), 245–253. https://doi.org/10.1002/jbm.b.30535.

Minitab, I., 2020. Version: Minitab® 20.2 (64-bit). MINITAB, Pennsylvania, USA [Internet]. http://www.minitab.com/en-US/products/minitab/.

Murphy, S.V., Atala, A., 2014. 3D bioprinting of tissues and organs. Nat. Biotechnol. 32 (8), 773–785. Available from: : http://www.nature.com/doifinder/10.1038/nbt.2958.

Nasircilar, A., Bulbul, M.V., Kalender, S.M., Bozkurt, C., Keskin, I., 2022. Effects of polyacrylamide hydrogel used in the treatment of osteoarthritis on mesenchymal stem cells and human osteoblasts. JOSAM 6 (4), 498–502. https://doi.org/10.28982/josam.1006577.

Patra, S., Ajayan, P.M., Narayanan, T.N., 2020. Dynamic mechanical analysis in materials science: the novice's tale. Open Mater. Sci. 1 (1) https://doi.org/10.1093/oxfmat/itaa001.

Sadeghi, H., Espino, D.M., Shepherd, D.E.T., 2015. Variation in viscoelastic properties of bovine articular cartilage below, up to and above healthy gait-relevant loading frequencies. Proc. Inst. Mech. Eng. H 229 (2), 115–123. https://doi.org/10.1177/0954411915570372.

Schwartz, C.J., Bahadur, S., 2007. Investigation of articular cartilage and counterface compliance in multi-directional sliding as in orthopedic implants. Wear 262 (11–12). https://doi.org/10.1016/j.wear.2007.01.007, 1315–20.

Stammen, J.A., Williams, S., Ku, D.N., Guldberg, R.E., 2001. Mechanical properties of a novel PVA hydrogel in shear and unconfined compression. Biomaterials 22 (8), 799–806. https://doi-org.bham-ezproxy.idm.oclc.org/10.1016/S0142-9612(00)00242-8.

Su, W., Hu, Y., Zeng, M., Li, M., Lin, S., Zhou, Y., et al., 2019. Design and evaluation of nano-hydroxyapatite/poly(vinyl alcohol) hydrogels coated with poly(lactic-co-glycolic acid)/nano-hydroxyapatite/poly(vinyl alcohol) scaffolds for cartilage repair. J. Orthop. Surg. Res. (446), 14. https://doi.org/10.1186/s13018-019-1450-0.

Uribe-Lam, E., Treviño-Quintanilla, C.D., Cuan-Urquizo, E., Olvera-Silva, O., 2021. Use of additive manufacturing for the fabrication of cellular and lattice materials: a review. Mater. Manuf. 36 (3), 257–280. https://doi.org/10.1080/10426914.2020.1819544.

Wan, W.K., Campbell, G., Zhang, Z.F., Hui, A.J., Boughner, D.R., 2002. Optimizing the tensile properties of polyvinyl alcohol hydrogel for the construction of a bioprosthetic heart valve stent. J. Biomed. Mater. Res. 63 (6), 854–861. https://doi-org.bham-ezproxy.idm.oclc.org/10.1002/jbm.10333.

Weems, A.C., Arno, M.C., Yu, W., Huckstepp, R.T., Dove, A.P., 2021. 4D polycarbonates via stereolithography as scaffolds for soft tissue repair. Nat. Commun. (1), 12. https://doi.org/10.1038/s41467-021-23956-6.

Wong, C.-H., Chen, C.-H., Chiu, L.-H., Tsuang, Y.-H., Bai, M.-Y., Chung, R.-J., et al., 2017. Facilitating in vivo articular cartilage repair by tissue-engineered cartilage grafts produced from auricular chondrocytes. Am. J. Sports Med. 46 (3), 713–728. https://doi-org.bham-ezproxy.idm.oclc.org/10.1177/0363546517741306.